



Expanded analysis of high-grade astrocytoma with piloid features identifies an epigenetically and clinically distinct subtype associated with neurofibromatosis type 1

Patrick J. Cimino¹ · Courtney Ketchum² · Rust Turakulov² · Omkar Singh² · Zied Abdullaev² · Caterina Giannini³ · Peter Pytel⁴ · Giselle Yvette Lopez⁵ · Howard Colman⁶ · MacLean P. Nasrallah⁷ · Mariarita Santi⁸ · Igor Lima Fernandes⁹ · Jeff Nirschl¹⁰ · Sonika Dahiya¹¹ · Stewart Neill¹² · David Solomon¹³ · Ellis Perez¹⁴ · David Capper¹⁴ · Haresh Mani¹⁵ · Dario Caccamo¹⁶ · Matthew Ball¹⁷ · Michael Badruddoja¹⁸ · Rati Chkheidze¹⁹ · Sandra Camelo-Piragua²⁰ · Joseph Fullmer²¹ · Sanda Alexandrescu²² · Gabrielle Yeane²³ · Charles Eberhart²⁴ · Maria Martinez-Lage²⁵ · Jie Chen²⁶ · Leor Zach²⁷ · B. K. Kleinschmidt-DeMasters²⁸ · Marco Hefti²⁹ · Maria-Beatriz Lopes³⁰ · Nicholas Nuechterlein³¹ · Craig Horbinski³² · Fausto J. Rodriguez³³ · Martha Quezado² · Drew Pratt² · Kenneth Aldape²

Received: 9 September 2022 / Revised: 16 October 2022 / Accepted: 16 October 2022 / Published online: 22 October 2022
This is a U.S. Government work and not under copyright protection in the US; foreign copyright protection may apply 2022

Abstract

High-grade astrocytoma with piloid features (HGAP) is a recently recognized glioma type whose classification is dependent on its global epigenetic signature. HGAP is characterized by alterations in the mitogen-activated protein kinase (MAPK) pathway, often co-occurring with *CDKN2A/B* homozygous deletion and/or *ATRX* mutation. Experience with HGAP is limited and to better understand this tumor type, we evaluated an expanded cohort of patients ($n = 144$) with these tumors, as defined by DNA methylation array testing, with a subset additionally evaluated by next-generation sequencing (NGS). Among evaluable cases, we confirmed the high prevalence *CDKN2A/B* homozygous deletion, and/or *ATRX* mutations/loss in this tumor type, along with a subset showing *NF1* alterations. Five of 93 (5.4%) cases sequenced harbored *TP53* mutations and RNA fusion analysis identified a single tumor containing an *NTRK2* gene fusion, neither of which have been previously reported in HGAP. Clustering analysis revealed the presence of three distinct HGAP subtypes (or groups = g) based on whole-genome DNA methylation patterns, which we provisionally designated as gNF1 ($n = 18$), g1 ($n = 72$), and g2 ($n = 54$) (median ages 43.5 years, 47 years, and 32 years, respectively). Subtype gNF1 is notable for enrichment with patients with Neurofibromatosis Type 1 (33.3%, $p = 0.0008$), confinement to the posterior fossa, hypermethylation in the *NF1* enhancer region, a trend towards decreased progression-free survival ($p = 0.0579$), RNA processing pathway dysregulation, and elevated non-neoplastic glia and neuron cell content ($p < 0.0001$ and $p < 0.0001$, respectively). Overall, our expanded cohort broadens the genetic, epigenetic, and clinical phenotype of HGAP and provides evidence for distinct epigenetic subtypes in this tumor type.

Keywords HGAP · High-grade astrocytoma with piloid features · NF1 · Neurofibromatosis type 1 · DNA Methylation

Introduction

High-grade astrocytoma with piloid features (HGAP) is a recently discovered and codified brain tumor type whose classification is dependent on its global DNA methylation signature [22]. These tumors can occur throughout the neuraxis, but are often located within the posterior fossa [21, 22]. The histopathology of HGAPs variably demonstrates lower-grade or higher-grade features, with characteristics overlapping those of pilocytic astrocytoma and glioblastoma

Patrick J. Cimino and Courtney Ketchum have contributed equally.

✉ Patrick J. Cimino
pj.cimino@nih.gov

✉ Kenneth Aldape
kenneth.aldape@nih.gov

Extended author information available on the last page of the article

[3, 22]. HGAPs are IDH-wildtype and frequently contain alterations in the mitogen-activated protein kinase (MAPK) pathway, in combination with homozygous deletion of *CDKN2A/B* and/or *ATRX* mutations [22]. While these genetic alterations may be characteristic, they are not specific to HGAP. What is unique to HGAP is its epigenetic profile; indeed, DNA methylation profiling is required for the definitive diagnosis of HGAP [4, 12]. Definitive diagnosis of HGAP is important for prognostic considerations, where its overall survival is between that of pilocytic astrocytoma (CNS WHO grade 1) and glioblastoma, IDH-wildtype (CNS WHO grade 4) [22]. The discovery of HGAP exemplifies the utility of identifying novel tumor entities through DNA methylation profiling [18, 22, 27]. DNA methylation profiling and clustering analysis are additionally useful for intra-class subtyping across numerous CNS tumor types [4, 16, 19, 28, 30]. Although HGAP was recently incorporated into the 2021 fifth edition of the World Health Organization Classification for Central Nervous System Tumors [12], there is incomplete understanding of this tumor type as there is a general lack of large published HGAP cohort studies [3, 22]. In this study, we sought to validate previously described aspects of HGAP as well as identify potential epigenetic subtypes that may have associated clinical implications.

Materials and methods

Tissue samples and datasets

The use of human subject material was performed in accordance with the World Medical Association Declaration of Helsinki and with the approval of the participating Institutional Review Boards. This study included (1) previously described cases of anaplastic astrocytoma with piloid features [3, 22], (2) cases from the Laboratory of Pathology clinical consult service at the National Institutes of Health (NIH) in Bethesda, MD, USA and (3) other published cases with available methylation array data in the form of raw IDAT files. Referral consult cases were received from the following institutions: Mayo Clinic (Rochester, Minnesota); University of Michigan Medical Center (Ann Arbor, Michigan); University of California San Francisco Medical Center (San Francisco, California); Barnes Jewish Hospital (St. Louis, Missouri); Children's Hospital of Philadelphia (Philadelphia, Pennsylvania); Hospital of the University of Pennsylvania (Philadelphia, Pennsylvania); Duke University Medical Center (Durham, North Carolina); Laboratorio Bacchi (Sao Paulo, Brazil); Stanford University Medical Center (Palo Alto, California); University of Chicago Medical Center (Chicago, Illinois); Beaumont Hospital (Royal Oak, Michigan); Boston Children's Hospital (Boston, Massachusetts); Brigham and Women's Hospital (Boston,

Massachusetts); Cleveland Clinic (Cleveland, Ohio); Emory University Hospital (Atlanta, Georgia); Inova Fairfax Hospital (Falls Church, Virginia); Intermountain Central Laboratory (Murray, Utah); Johns Hopkins Hospital (Baltimore, Maryland); Massachusetts General Hospital (Boston, Massachusetts); Mercy General Hospital (Sacramento, California); University of Nebraska Medical Center (Omaha, Nebraska); Northwestern Memorial Hospital (Chicago, IL); Sheba Medical Center (Tel Hashomer, Israel); Tucson Medical Center (Tucson, Arizona); University of California Los Angeles Medical Center (Los Angeles, California); University of Alabama (Birmingham, Alabama); University of Colorado Hospital (Aurora, Colorado); University of Iowa Hospitals (Iowa City, Iowa); ARUP Laboratories (Salt Lake City, Utah); and the University of Virginia Health System (Charlottesville, Virginia). Each of the 61 referral consult cases was reviewed for histopathology as part of the diagnostic process by at least two board-certified neuropathologists (PJC, MQ, DP, KA). When available, we noted clinical features including subject demographics, tumor location, surgical procedure (biopsy versus excision—subtotal versus gross total was not available), and tumor occurrence (primary versus recurrence). Accompanying treatment modalities (chemotherapy and radiation) were not available. We defined progression-free survival as the duration from surgery of initial tumor to the date of clinical-radiographic progression or date of second resection for clinically/radiographically-determined tumor progression. Similarly, overall survival was defined as the duration from surgery of the initial tumor to death. These definitions were applied uniformly throughout our cohort. Cases were also extracted from publicly available methylation datasets included E-MTAB-5552 [14], GSE109381 [4], GSE143843 [11], GSE157397 [7], GSE175543 [6], Children's Brain Tumor Network (<https://cbtn.org>), and The Cancer Genome Atlas (<https://gdc.cancer.gov>).

DNA methylation array profiling

For institutional samples, tumor cellularity was confirmed to comprise at least 60% of the tissue. Genomic DNA was extracted from Formalin-Fixed Paraffin-Embedded (FFPE) tissue and underwent bisulfite-conversion (EZ DNA Methylation Kit, Zymo Research D5001) and restoration (Infinium FFPE DNA Restore kit, Illumina, USA). The DNA was then assayed on the Infinium MethylationEPIC kit (Illumina, USA) according to the Infinium HD FFPE Methylation Assay automated protocol (Illumina, USA). Raw idat files were used for classification using version 11b6 of the Heidelberg methylation-based classifier [4]. Cases which received a primary methylation class designation of anaplastic pilocytic astrocytoma, (the original class designation for the HGAP WHO tumor type) and had other features

consistent with this glial tumor (such as astrocytic histomorphology, glial fibrillary acidic protein immunopositivity, and/or Olig2 immunopositivity), were included for analysis in this study. Glial features were confirmed centrally and independently by at least two board-certified neuropathologists (PJC, MQ, DP, KA).

Bioinformatic analyses

Microarray idat files were processed with functional normalization using the meffil package [15]. This R package is available from Bioconductor (<https://www.bioconductor.org/>) and GitHub (<https://github.com/perishky/meffil>). Functional normalization was performed with the meffil package, which is based on linear regression modelling [15]. The quantile normalization runs an inbuilt algorithm based on illumina control probes. This model removes control probe variance from the sample quantiles and simultaneously adjusting probe intensities for additional fixed and random effects. Those fixed and random effects variables supplied to normalization function and coded from the metadata we collected for all samples. We choose type of array variables (HumanMethylation450 vs MethylationEPIC BeadChip) and tissue preservation method (Frozen vs FFPE) as fixed effect and also included random effect attributed to individual chip barcode. Random effects are handled in meffil by using the lme4 R package [2]. The meffil package provided automated estimation of functional normalization parameters to compensate for chip to chip (barcode) variance.

For unsupervised hierarchical clustering, the most significant probes were clustered and plotted with ComplexHeatmap package available through Bioconductor [9]. This package allows hierarchical cluster with different methods for columns and rows. We used default “euclidean” metrics for distance matrix and “average” for the dendrogram construction. Normalized beta values were filtered to the most differentially methylated probes calculated by student t-test contrasting each group pairs: Group1 vs Group2, Group1 vs gNF1, Group2 vs gNF1. Bonferroni correction was applied to p-values and 772 probes with p-value below 0.05 were selected for heat map and Uniform Manifold Approximation and Projection (UMAP) plots. UMAP plot was produced with r package uwot: The Uniform Manifold Approximation and Projection (UMAP) Method for Dimensionality Reduction (<https://arxiv.org/abs/1802.03426>). We used two methods to estimate tumor ratio and cell composition in each sample: meffil package described above and the CIBERSORT package (<https://cibersortx.stanford.edu/>). Both methods showed good correlation with each other. The meffil package supplied prebuild reference “guintivano dlpc” for the brain tissue deconvolution with five cell types. Those reference profiles were based on published Bioconductor package FlowSorted.DLPFC.450 k. (<https://github.com/>

[perishky/meffil/wiki/Estimating-cellular-composition](https://github.com/perishky/meffil/wiki/Estimating-cellular-composition)). Signature matrices were used to determine neoplastic cell and various tumor microenvironment cell fractions through methylCIBERSORT as previously described [25]. The r package methylGSA was used for gene ontology pathway analysis [23].

Targeted next-generation DNA sequencing

For cases with available DNA, next generation sequencing (NGS) data were obtained as previously described using either a custom amplicon-based brain tumor specific panel [20] or a commercial panel TruSight Oncology 500 (TSO 500; Illumina, San Diego, USA) [18]. The TSO 500 panel genes are available on the manufacturer’s website (<https://www.illumina.com/products/by-type/clinical-research-products/trusight-oncology-500.html>). Illumina platform libraries were prepared using TSO 500 kit according to the manufacturer’s protocol. Amplified pre-enriched libraries were hybridized to probes specific to the TSO 500 targeted gene panel. Enriched libraries were amplified, quantified, normalized, and sequenced as paired-end reads on a high-output NextSeq 500/550 flow cell. The TSO 500 local app was used for alignment and variant calling. Variants were manually reviewed by visual inspection of the raw sequencing read alignments using the Integrative Genomics Viewer [24]. For a subset of cases, sequencing was obtained from publicly available sources or performed at the outside referring institutions and those results were reported as part of the consultation process (sources of sequencing summarized in Supplemental Table 1). For previously described HGAP cases [22], sequencing data were obtained from the authors.

Statistics

Statistical analyses were performed using R software (Version 3.3.2, RProject for Statistical Computing, <http://www.r-project.org/>). Kaplan–Meier analysis for survival, correlation matrix analysis, and principal component analysis were performed using GraphPad Prism software (Version 7.02, <https://www.graphpad.com/scientific-software/prism>). For direct comparisons between groups, Mann–Whitney U test was used unless otherwise indicated. Chi-squared test was performed to compare frequencies across groups.

Results

Expanded HGAP demographics, histologic features, and genetic characteristics

Our total cohort was composed of 148 tumor samples from 144 patients (Supplemental Table 2). The mean and median

age of patients at the time of surgery were 44 years and 43 years (range 4–88 years), respectively. Of the 135 patients with known age at time of diagnosis, 12 (8.9%) were in the pediatric age group (< 18 years) (Supplemental Table 2). Tumors occurred in 59 female and 85 male patients (ratio 1:1.44). Disease stage included 74 primary tumors, 38 recurrent tumors, and 36 tumors with unknown designation. Tumor location was known for 130 patients, with 81 located in the posterior fossa, 34 located in the supratentorial region, and 13 in the spinal cord. Histopathology on available cases included glioblastoma-like histomorphology (Fig. 1a–f) and most with an infiltrative growth pattern, in 26 of the 30 (86.7%) evaluable cases. The presence of necrosis and/or microvascular proliferation was observed in 38 of 61 (62.3%) HGAP tumors. The piloid-associated features of Rosenthal fibers and/or eosinophilic granular bodies were present in a minority (23 of 61; 37.7%). Mitotic activity was variable, ranging from 0 to 6 mitoses/mm². Similarly, the maximum Ki-67 proliferative index had a broad spectrum, ranging 1–30%.

The most frequent genetic alterations were in the *Cyclin Dependent Kinase Inhibitor 2A (CDKN2A)*, *Alpha Thalassemia/mental Retardation syndrome, X-linked (ATRX)* and *Neurofibromin 1 (NF1)* genes, consistent with previous findings of HGAP [22] (Supplemental Table 1). *CDKN2A* was the most commonly altered gene (121/144, 84.1%). *ATRX* status, as determined either by DNA sequencing or surrogate immunohistochemistry, was known for 111

cases, of which 65 (58.6%) were mutated or lost. *NF1* was the most frequently altered gene of the MAPK pathway. *NF1* was sequenced in 89 cases, with a mutation identified in 36 (40.4%). *FGFR1* was the second most frequently altered MAPK pathway gene, with 17 of the 89 cases sequenced for *FGFR1* harboring a mutation (19.1%), and an additional 6 of 43 (14.0%) tested cases harboring fusions of *FGFR1* (Supplemental Table 1). *BRAF* is another MAPK pathway gene for which mutations/fusions were nearly as common as *FGFR1* alterations. There were 18 cases of 97 (18.6%) tested which harbored a *BRAF* fusion, and 2 cases of 86 (2.3%) sequenced were *BRAF*-V600E mutant. *KRAS* was a less frequently altered gene of the MAPK pathway, with a mutation identified in 1 of 91 (1.1%) samples tested. The overall composition of MAPK alterations in our HGAP cohort ($n = 144$), were as follows: $n = 79$ with one reported MAPK alteration, $n = 8$ with two or more MAPK alterations, $n = 33$ without a detected alteration, and $n = 24$ with no genomic testing results available (Supplemental Table 1). A *TERT* promoter mutation was identified in 1 of 93 (1.1%) tumors and was mutually exclusive of *ATRX* loss. Sequencing revealed genetic alterations not yet reported in HGAP, including *TP53* mutations and a *KANK2::NTRK2* fusion. *TP53* mutation status was available for 93 cases, of which 5 (5.4%) contained pathogenic mutations as determined by DNA sequencing. Immunohistochemistry was not used in our evaluation of p53 status.

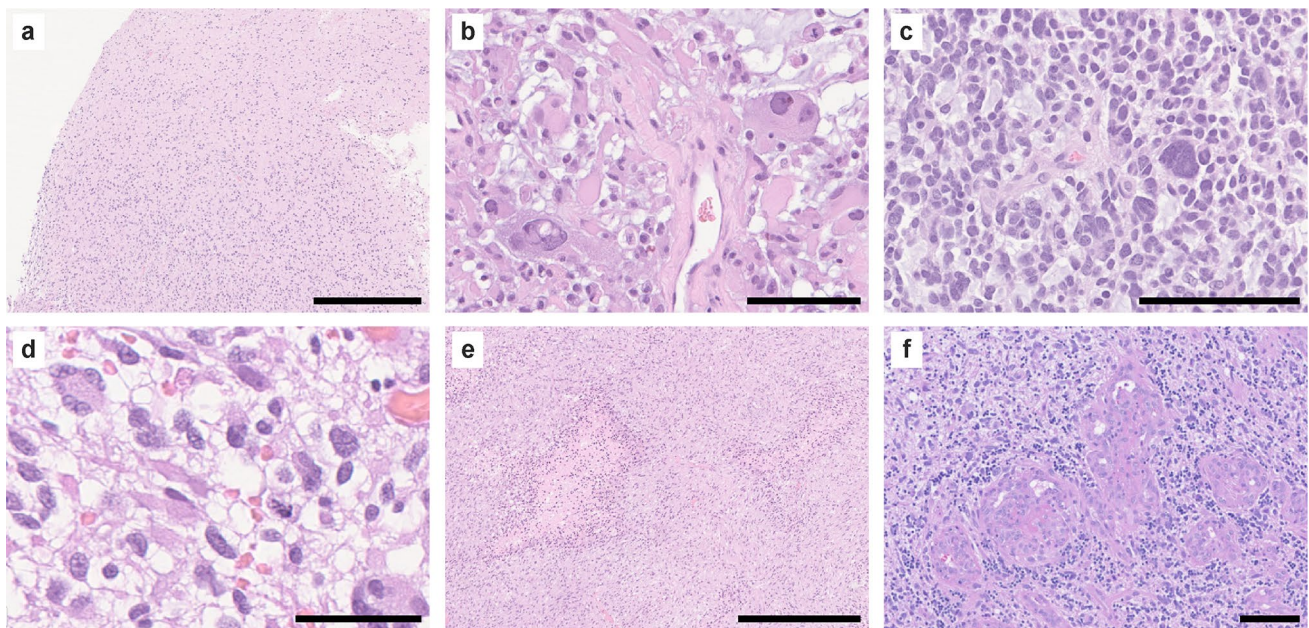


Fig. 1 Representative high-grade histologic features frequently present in HGAP. **a** HGAP tumors often had an infiltrative growth pattern. **b, c** Tumors repeatedly demonstrated pleomorphism and/or poorly differentiated cytomorphologies. **d** Increased mitotic activity

occurred in a subset of cases. **e** Palisading necrosis and/or **f** microvascular proliferation were present in a majority of HGAP tumors. (Scale bars: **a** 500 μ m, **b** 100 μ m, **c** 100 μ m, **d** 50 μ m, **e** 500 μ m, **f** 100 μ m)

HGAP epigenetic subtyping with relevant clinical features

Analyzing whole-genome DNA methylation for multiple glial/glioneuronal tumor types, we confirmed our classifier results in which HGAP forms a distinct tumor type by unsupervised Uniform Manifold Approximation and Projection (UMAP) (Fig. 2A) and unsupervised hierarchical clustering (Supplemental Fig. 1). To identify potential distinct HGAP epigenetic subtypes in an unbiased fashion, we started with unsupervised hierarchical clustering analysis. This clustering led to the identification of three distinct HGAP epigenetic subtypes (Fig. 2b, Supplemental Fig. 2). Cluster subtyping was further supported by unsupervised dimensionality reduction using UMAP analysis (Fig. 2c). The smallest of the three groups ($n = 18$, 12.5%) was observed to contain a relatively high proportion of patients with a clinical diagnosis of Neurofibromatosis Type 1 (NF1) ($p = 0.0008$), and therefore this subtype was designated as group NF1 (gNF1) (Figs. 2, 3a). The other two subtypes were designated simply as Group 1 (g1; $n = 72$, 50.0%) and Group 2 (g2; $n = 54$, 37.5%). Although the gNF1 was enriched for patients with germline alterations, there was no difference in the frequency of *NF1* alterations detected in the tumors across subtypes (Fig. 3b). However, given the fact that hypermethylation of the *NF1* promoter region may be an alternate mechanism for NF1 inactivation [10], we evaluated for potential *NF1* methylation differences across the three HGAP subtypes. Indeed, 5 of 30 (16.7%) of the CpG probes related to *NF1* were differentially methylated in gNF1 when compared to the other subtypes (Fig. 3c).

Several clinical features beyond NF1 status tended to differ across HGAP subtypes. The initial tumors of gNF1, g1, and g2 subtypes had median ages of 43.5 years, 47.0 years, and 32.0 years, respectively ($p > 0.05$ for all pairwise comparisons, Mann–Whitney *U* tests, Fig. 4a, b). Only one of the twelve pediatric tumors was gNF1 subtype (Supplemental Table 2). Tumor localization varied among the three HGAP subtypes, with gNF1 having 100% of the tumors located in the posterior fossa (Fig. 4c, d). By contrast, subtypes g1 (35.4% supratentorial, 55.4% posterior fossa, 9.2% spinal cord) and g2 (29.2% supratentorial, 56.2% posterior fossa, 14.6% spinal cord) were found throughout the neuraxis (Fig. 4d). While HGAP subtype was associated with tumor location (chi-square, $**p = 0.001$) the significance was less than that of subtype association with NF1 syndrome. Furthermore, no association was observed between tumor location and NF1 syndrome ($p = 0.359$). Tumor location itself was not associated with difference in survival (Supplemental Fig. 3). Progression-free survival trended towards worse outcome for the gNF1 subtype when compared to the other two subtypes (Fig. 4e, f). The gNF1, g1, and g2 subtypes had median progression-free survival times of 252 days,

565 days, and 618 days, respectively. Overall survival appeared similar among all subtypes, although the number of patients with overall survival data was low (Fig. 4g, h). Three of the patients had recurrent tumors, all of which maintained their subtype assignment when compared to their original tumor. The first of these three patients had known Neurofibromatosis Type 1, with their original and two recurrent HGAPs all belonging to the gNF1 HGAP subtype. The other two patients did not have a clinical diagnosis of Neurofibromatosis Type 1. The second patient had paired initial and recurrent HGAP tumor in the g1 subtype while the third patient had paired initial and recurrent HGAP tumor in the g2 subtype.

HGAP subtype specific genetic, epigenetic, and tumor microenvironment features

In addition to *NF1* alterations already discussed, we evaluated subtype-specific genetic changes in the other commonly altered genes *ATRX* and *CDKN2A/B*, as well as the novel *TP53* mutants and *NTRK2* gene fusion. *ATRX* alterations (as determined by immunohistochemistry and/or sequencing) were overrepresented ($p = 0.023$) in the gNF1 subtype (87.5%) when compared to the g1 and g2 groups (59.6% and 47.5%, respectively) (Fig. 3b). No difference in *CDKN2A/B* deletion status was observed across HGAP subtypes ($p = 0.949$), with all subtypes having a high frequency of alterations (gNF1 = 84.2%, g1 = 83.3%, g2 = 85.5%) (Fig. 3b). Of the five novel *TP53* mutant cases we found, four were present in the g1 subtype, one was in g2, and none were found in the gNF1 subtype. The sole *NTRK2* gene fusion positive HGAP was present in the g2 subtype.

Given the clinical and genetic relevance of the gNF1 subtype so far, we sought to interrogate global epigenetic changes to uncover potential underlying biological pathways specifically related to the gNF1 subtype when compared to the other subtypes. First, we performed differential methylation analysis for two separate comparisons, gNF1 versus g1 and gNF1 versus g2 (Fig. 5a, Supplemental Table 3). Then we filtered for the significantly altered genes shared between both comparison lists. Next, we performed MethylGSA for Gene Ontology (GO) analysis. When we look at all gene probes in all gene structure sites, six of the top ten pathways that are relatively dysregulated in the gNF1 subtype involve RNA processes (RNA methylation, RNA methyltransferase activity, DNA-directed RNA polymerase complex, RNA polymerase complex, nuclear DNA-directed RNA polymerase complex, and RNA polymerase II holoenzyme) while the last four processes involve protein regulation (histone deacetylase complex, protein acetylation, protein deubiquitylation, protein modification by small protein removal) (Fig. 5b). Next, we sought to understand what portion of the gene structure (promoter versus gene body)

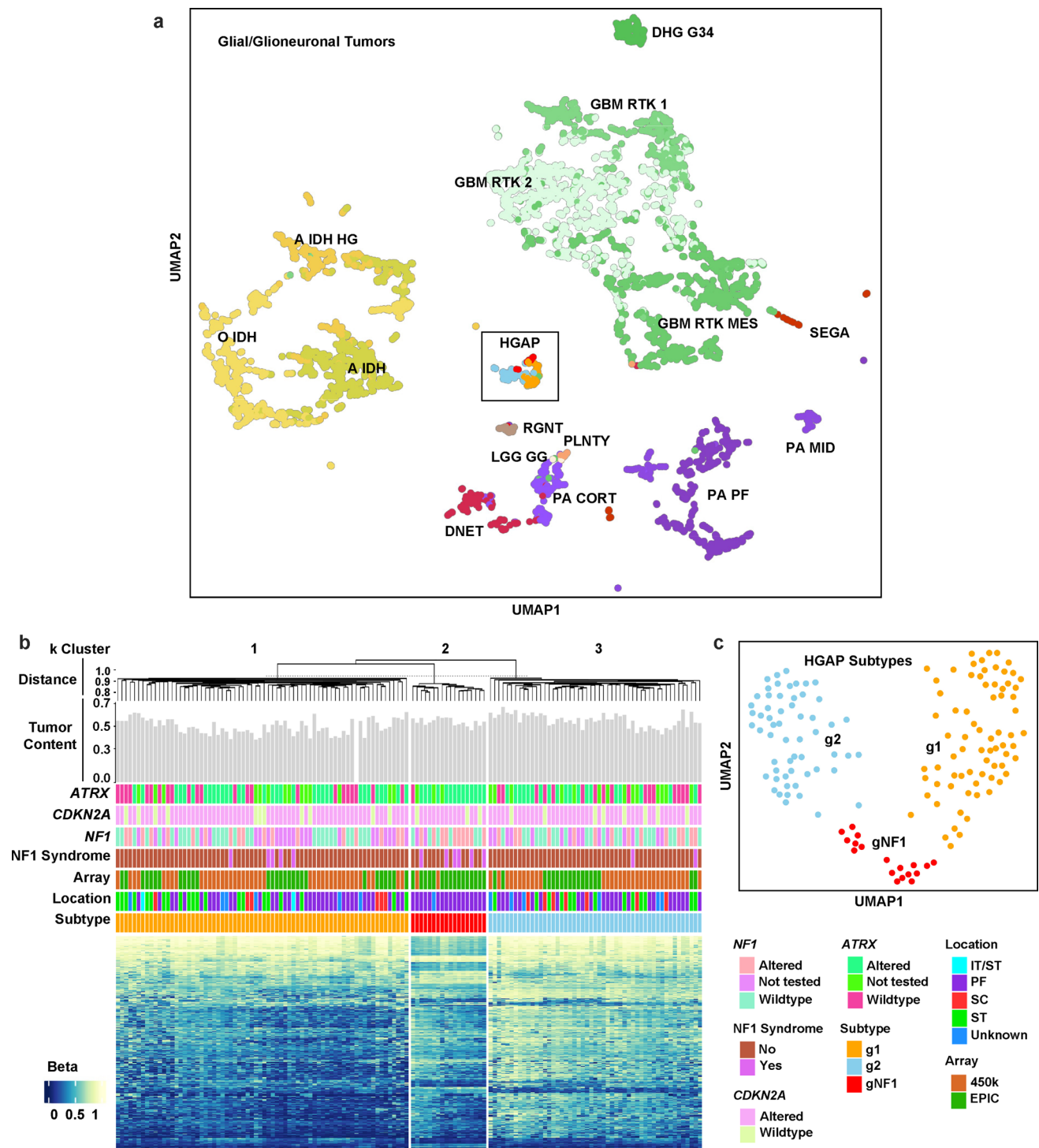


Fig. 2 HGAP resolves into three epigenetically determined subtypes. **a** Uniform Manifold Approximation and Projection (UMAP) dimensionality reduction confirms that HGAP forms a distinct methylation cluster when compared to other CNS glial/glioneuronal tumors. **b** Unsupervised hierarchical clustering heatmap of whole-genome CpG

methylation for HGAP uncovers the presence of three distinct HGAP epigenetic subtypes. **c** UMAP dimensionality reduction of HGAP only confirms the presence of three HGAP subtypes. *IT* Infratentorial, *ST* supratentorial, *PF* posterior fossa, *SC* spinal cord)

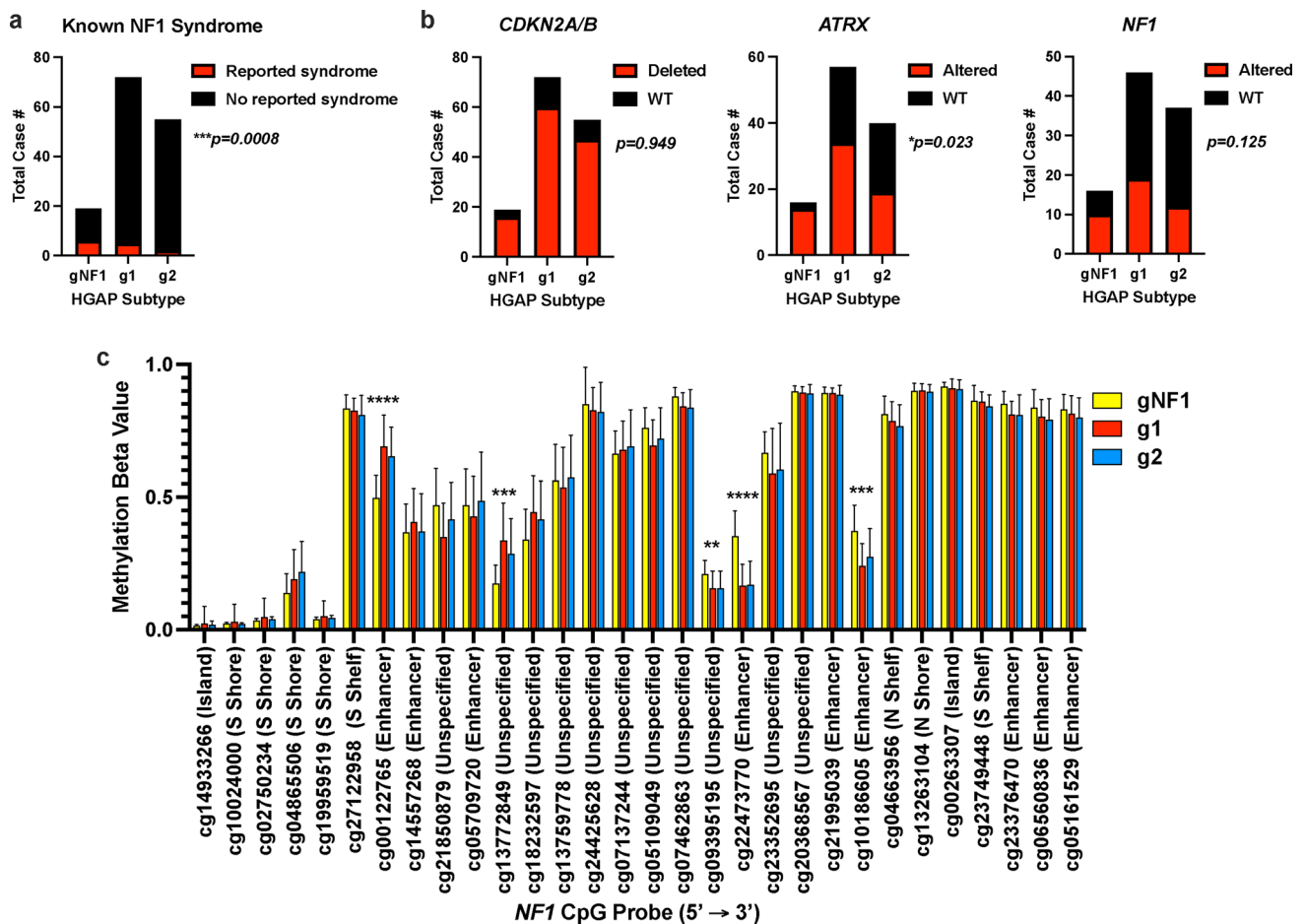


Fig. 3 *NF1* germline status, somatic alterations, and *NF1* methylation define a relevant HGAP subtype. **a** HGAP subtype gNF1 is enriched for patients having Neurofibromatosis Type 1 (*NF1*) (gNF1=33.3%, g1=6.9%, g2=3.6%) and **bATRAX alterations (gNF1=87.5%, g1=59.6%, g2=47.5%). **b** *CDKN2A/B* (gNF1=83.3%, g1=83.3%,**

g2=85.5%) and *NF1* (gNF1=62.5%, g1=41.3%, g2=32.4%) alterations are common across HGAP subtypes. **c** There are 5 of 30 (16.7%) CpG probes in the *NF1* regulatory region that are differentially methylated in the gNF1 subtype, 3 of which are in the gene enhancer region

was responsible for the differential methylation signature related to the RNA pathway dysregulation in gNF1 (Fig. 5c). To do this, we made multiple comparisons of CpG probes that were either relatively hypermethylated or hypomethylated in the gNF1 subtype. Of these comparisons, there were no dysregulated RNA processing pathways in the top ten pathways found in the promoter 1 (TSS1500 + TSS200) or promoter 2 (TSS1500 + TSS200 + 5' UTR + EXON 1) regions (Fig. 5d, Supplemental Fig. 4). In contrast, three of the top ten pathways in gNF1 hypermethylated gene bodies (coding region), as well as three of the top ten pathways in gNF1 hypomethylated gene bodies, involved RNA processing pathways. Overall, this indicates an association between both hypermethylation and hypomethylation of gene bodies and dysregulation of RNA processing pathways in the gNF1 subtype.

Given the important contribution of the tumor microenvironment (TME) to tumor biology, we sought to understand

the cellular composition of HGAP and its subtypes. To do this, we began by performing methylCIBERSORT [25] for deconvolution of cell type components, both neoplastic and non-neoplastic, from the whole-genome methylation data. For HGAP overall as a tumor type, we found positive correlations between monocytes and B cells ($r=0.56$), NK cells and B cells ($r=0.48$), and neurons and glia ($r=0.47$) (Fig. 6a). These TME cell associations were further confirmed with principal component analysis (Fig. 6b). Next, we analyzed tumor content in a subtype specific manner, beginning with the neoplastic cell component. Subtypes gNF1 and g1 had a lower neoplastic cell content (higher TME cell component) when compared to g2 ($p=0.0055$ and $p<0.0001$, respectively) (Fig. 6c). When looking at the non-neoplastic cells, g1 and gNF1 appear to have unique signatures. Subtype g1 is enriched for monocytes when compared to gNF1 ($p<0.0001$) and g2 ($p<0.0001$) (Fig. 6d, e). In partial alignment with the monocytes and B cells being

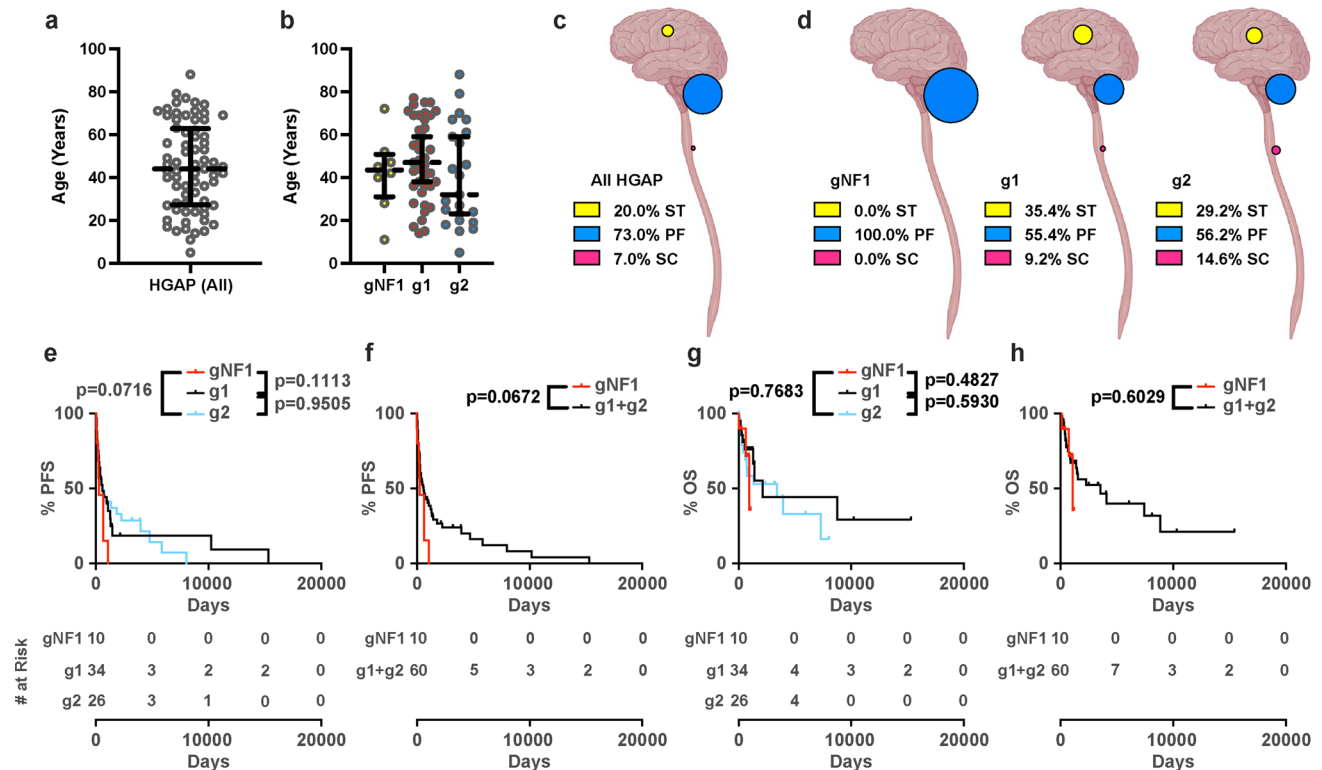


Fig. 4 Clinical features of HGAP methylation subtypes. Median age with interquartile range for **a** all HGAPs and **b** HGAP subtypes ($p > 0.05$ for all pairwise comparisons, Mann–Whitney U tests). Localization for **c** all HGAP tumors and **d** HGAP by subtype

(*ST* supratentorial, *PF* posterior fossa, *SC* spinal cord). Progression-free survival (PFS) with number at risk for **e** all HGAP subtypes and **f** gNF1 subtype versus the others. Overall survival (OS) with number at risk for **g** all HGAP subtypes and **h** gNF1 subtype versus the others

moderately correlated in HGAP, subtype g1 is also enriched in B cells when compared to gNF1 ($p = 0.0385$), but not when compared to g2 ($p = 0.1696$). The enriched immune cell component of subtype g1 does not appear associated with primary versus recurrent tumor status, as these occurrences (primary versus recurrence) do not differ across subtypes (Supplemental Table 4). Also consistent with the correlation matrix, subtype gNF1 is enriched for both neurons and glia when compared to subtypes g1 ($p < 0.0001$ each comparison) and g2 ($p < 0.0001$ each comparison) (Fig. 6d, e). Summarizing the TME component of HGAP subtypes, gNF1 is enriched for neurons and glia, g1 is enriched for monocytes and B cells, and g2 has the lowest amount of non-neoplastic TME content.

Discussion

The findings from our analysis of a large HGAP cohort has several clinical implications, especially related to tumor classification in general. We have confirmed and helped to solidify the concept that HGAPs are largely infiltrative glial neoplasms, often with glioblastoma-like histology (more so than pilocytic astrocytoma-like histology) and that future

WHO classification schemes may consider these features in its nosology [12]. Consideration as to whether the ‘piloid’ designation in HGAP is warranted, as this not reflective of the histology found in most tumors designated as HGAP by DNA methylation profiling. A name more neutral to histological features may be warranted, especially in this tumor type that is currently defined by its DNA methylation profile, not its histological features. DNA methylation profiling has been incorporated into essential or desirable diagnostic criteria for a substantial proportion of CNS tumors in the WHO “blue book” and it is therefore feasible to consider more widespread profiling of cases when HGAP is considered as a diagnostic possibility. DNA methylation profiling to rule out HGAP may be warranted, especially in cases of a cerebellar glial neoplasm that does not fit neatly into another WHO diagnostic category, where the index of suspicion rises in the setting of *ATRX* loss and/or *CDKN2A* homozygous deletion. Methylation testing may also be considered when other tumor features are suggestive of HGAP as well, such as a histologically high-grade glioma arising in the setting of Neurofibromatosis Type 1.

Beyond classification, there may also be clinical implications of HGAP subtyping according to distinct epigenetic subtypes. While gNF1 was the least frequent subtype, our

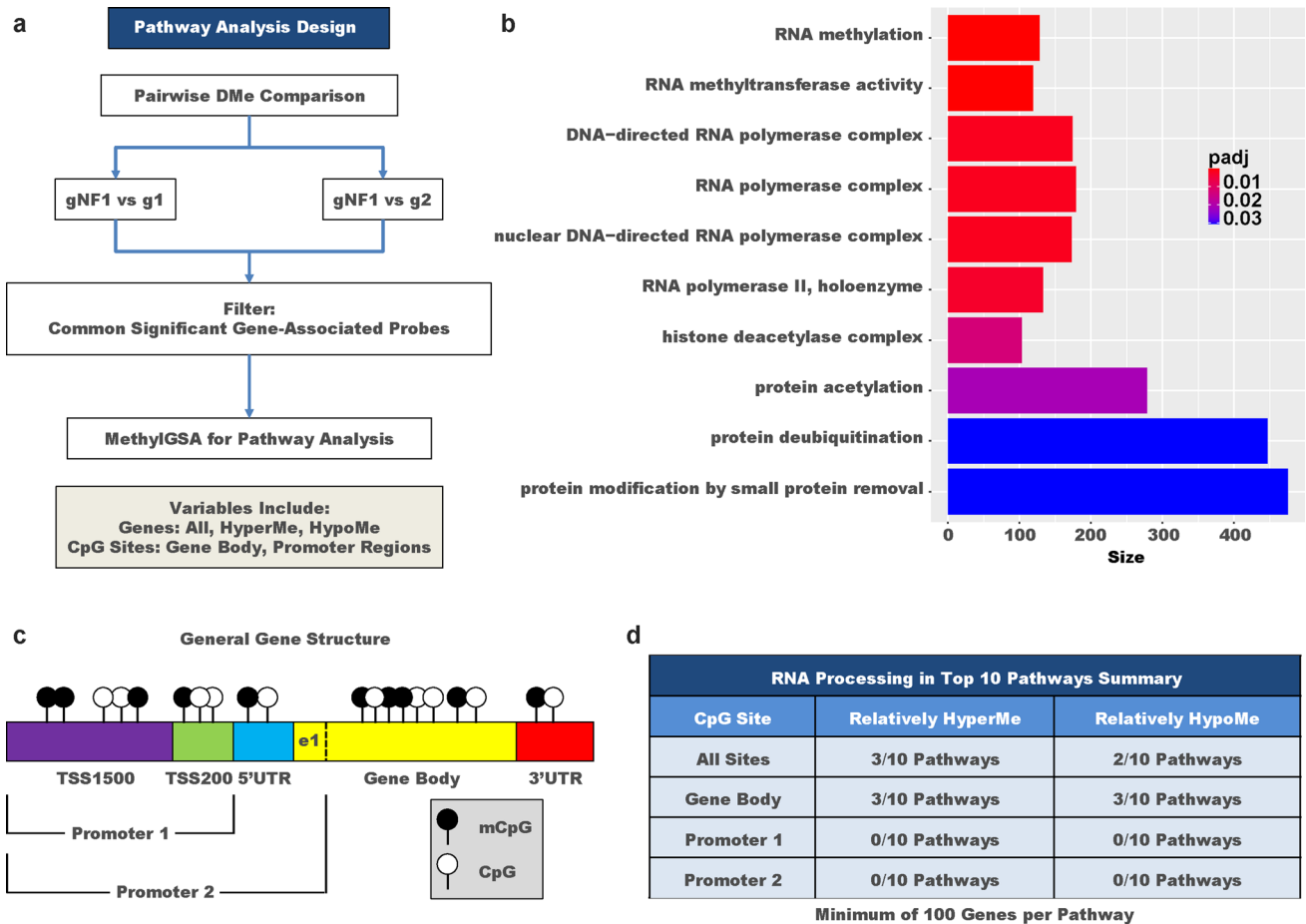


Fig. 5 Gene Ontology (GO) pathway analysis of HGAP subtypes. **a** Schematic for differentially methylated CpG probes between HGAP subtypes and downstream GO analysis. **b** Top 10 GO pathways that are dysregulated in gNF1 compared to other HGAP subtypes when utilizing all gene structure methylation sites for CpG sites that are

either hypermethylated or hypomethylated. **c** General gene structure of evaluated regions. **d** RNA processing dysregulation in the gNF1 subtype is a function of hypermethylation or hypomethylation in the gene body region, not promoter region of the associated genes

data indicates a trend towards a worse outcome than other HGAP subtypes. Furthermore, due to the overrepresented nature of NF1 occurring in the gNF1 subtype, HGAP subtyping analysis may point to the potential need for germline *NF1* testing for cases that fall into this class. Our findings are consistent with a recent report describing a larger proportion of HGAPs being found in a series of NF1-associated high-grade gliomas [13]. Methylation findings suggest that the gNF1 subtype may be associated with RNA processing dysregulation, which raises the possibility of this biological process acting as a potential therapeutic vulnerability in gNF1 HGAP, similar to other cancer types [8, 17, 26, 31]. In the future, it is possible that epigenetic subtyping may even be considered for the basis of biomarker-informed clinical trials including HGAP for proper risk stratification [1, 5, 29].

While this study represents a large cohort of patients with HGAP, it has some limitations, including those inherent to a retrospective study. Expanding the patient outcome data

would contribute to our understanding of the clinical heterogeneity and understanding of patterns of patient survival for this tumor type. additional helpful data would include surgical extent of resection and adjuvant treatment modalities for these patients. Additionally, next-generation sequencing data were obtained from a variety of different institutions with different gene region coverages, resulting in missing information for some genes. Therefore, it is difficult to know the exact mutational status for all genes of interest for every case in our cohort. We also lacked additional material for orthogonal validation of our biological investigations, such as immunohistochemistry for TME analysis and frozen tissue for high-quality RNA studies of RNA processing dysregulation. Further work is needed to more fully understand the clinical and biologic properties on this recently described tumor type.

In summary, we have characterized an expanded cohort of patients with HGAP by extending the spectrum of gene

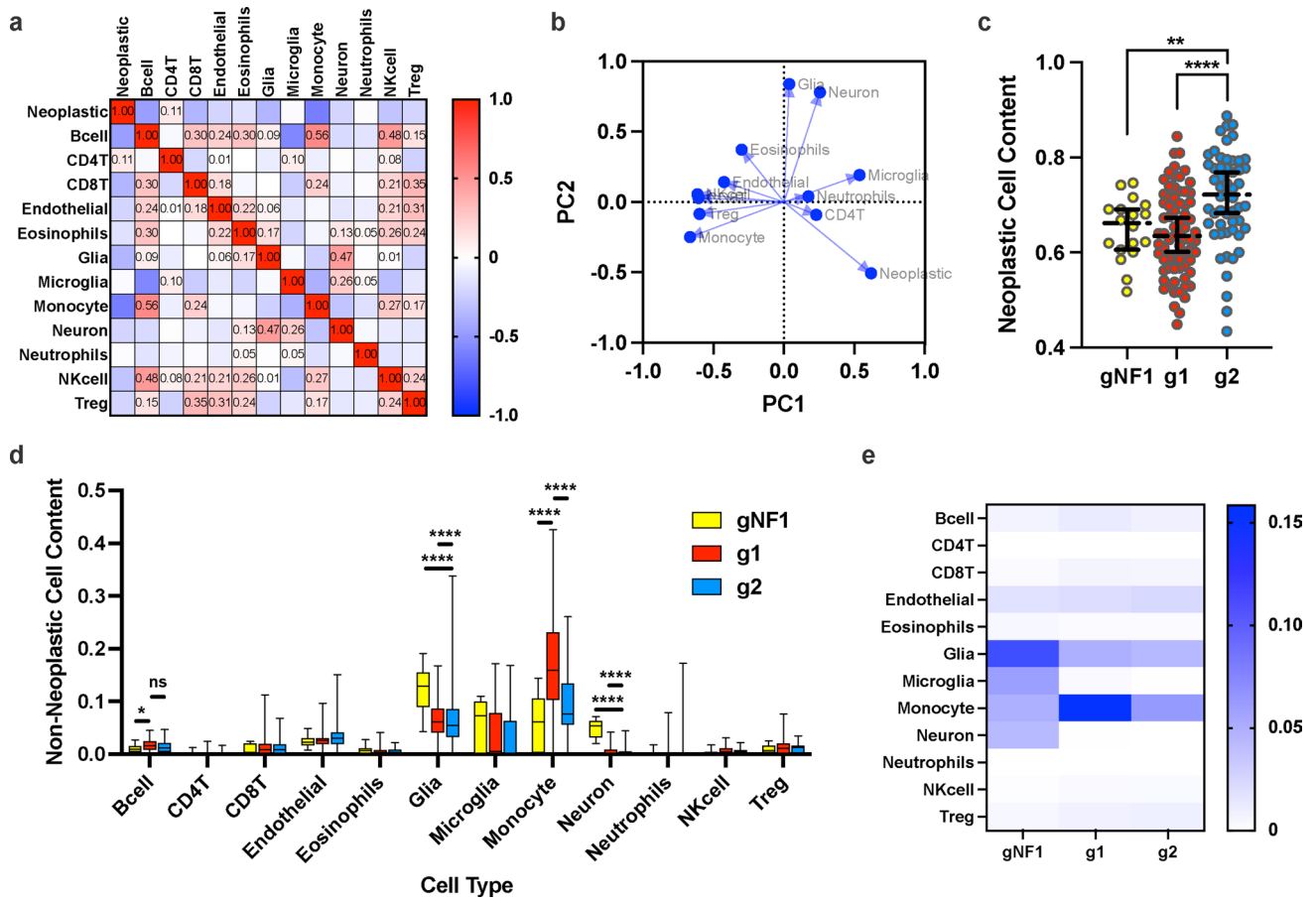


Fig. 6 Deconvolution of the tumor microenvironment in HGAP. **a** Correlation matrix and **b** principal component analysis of neoplastic and non-neoplastic cell components within HGAP as a single tumor type. **c** Neoplastic cell contents as a function of HGAP subtype, which is highest in the g2 subtype (error bars as median values

with 95% CI). **d** Non-neoplastic cell contents as a function of HGAP subtype, indicating that glia and neurons are enriched in the gNF1 subtype while monocytes and possibly B cells are enriched in the g1 subtype. **e** Heatmap summarizing the relative non-neoplastic cell contents in each HGAP subtype

alterations to include rare *TP53* mutations and an *NTRK2* fusion, highlighting that most tumors contain glioblastoma-like histological features, and uncovering the presence of three distinct epigenetic subtypes of HGAP. These HGAP epigenetic subtypes are associated with variations in clinical parameters, genetic alterations, and associated biological processes. Specifically, we identified an HGAP epigenetic subtype (provisionally designated here as gNF1) that is associated with enrichment for NF1 syndrome, increased *ATRX* alteration, increased methylation in the *NF1* enhancer region, evidence of RNA processing dysregulation, increased non-neoplastic glia and neuron cell content, and is confined to the posterior fossa with trends towards worse patient outcome. The goal of our work was to expand the understanding of a clinical and biological features of this recently described and understudied tumor type. Further work will likely elucidate additional biologic and clinical features of this newly defined CNS tumor type.

Supplementary Information The online version contains supplementary material available at <https://doi.org/10.1007/s00401-022-02513-5>.

Acknowledgements This work utilized the computational resources of the NIH HPC Biowulf cluster.

Funding This work was supported by the Intramural Research Program at the Center for Cancer Research, National Cancer Institute and the National Institute of Neurological Disorders and Stroke of the National Institutes of Health.

Declarations

Conflict of interest The authors declare that there are no conflicts of interest.

References


- Alexander BM, Trippa L, Gaffey S, Arrillaga-Romany IC, Lee EQ, Rinne ML et al (2019) Individualized Screening Trial of Innovative Glioblastoma Therapy (INSIGHT): a Bayesian

- adaptive platform trial to develop precision medicines for patients with glioblastoma. *JCO Precis Oncol*. <https://doi.org/10.1200/PO.18.00071>
2. Bates D, Machler M, Bolker B, Walker S (2015) Fitting linear mixed-effects models using lme4. *J Stat Softw* 67:1–48. <https://doi.org/10.18637/jss.v067.i01>
 3. Bender K, Perez E, Chirica M, Onken J, Kahn J, Brenner W et al (2021) High-grade astrocytoma with piloid features (HGAP): the Charite experience with a new central nervous system tumor entity. *J Neurooncol* 153:109–120. <https://doi.org/10.1007/s11060-021-03749-z>
 4. Capper D, Jones DTW, Sill M, Hovestadt V, Schrimpf D, Sturm D et al (2018) DNA methylation-based classification of central nervous system tumours. *Nature* 555:469–474. <https://doi.org/10.1038/nature26000>
 5. Cimino PJ, McFerrin L, Wirsching HG, Arora S, Bolouri H, Rabadan R et al (2018) Copy number profiling across glioblastoma populations has implications for clinical trial design. *Neuro Oncol* 20:1368–1373. <https://doi.org/10.1093/neuonc/noy108>
 6. DeSisto J, Lucas JT Jr, Xu K, Donson A, Lin T, Sanford B et al (2021) Comprehensive molecular characterization of pediatric radiation-induced high-grade glioma. *Nat Commun* 12:5531. <https://doi.org/10.1038/s41467-021-25709-x>
 7. Dodgshun AJ, Fukuoka K, Edwards M, Bianchi VJ, Das A, Sexton-Oates A et al (2020) Germline-driven replication repair-deficient high-grade gliomas exhibit unique hypomethylation patterns. *Acta Neuropathol* 140:765–776. <https://doi.org/10.1007/s00401-020-02209-8>
 8. Ferreira R, Schneekloth JS Jr, Panov KI, Hannan KM, Hannan RD (2020) Targeting the RNA polymerase I transcription for cancer therapy comes of age. *Cells*. <https://doi.org/10.3390/cells9020266>
 9. Gu Z, Eils R, Schlesner M (2016) Complex heatmaps reveal patterns and correlations in multidimensional genomic data. *Bioinformatics* 32:2847–2849. <https://doi.org/10.1093/bioinformatics/btw313>
 10. Gutmann DH, McLellan MD, Hussain I, Wallis JW, Fulton LL, Fulton RS et al (2013) Somatic neurofibromatosis type 1 (NF1) inactivation characterizes NF1-associated pilocytic astrocytoma. *Genome Res* 23:431–439. <https://doi.org/10.1101/gr.142604.112>
 11. Kessler T, Berberich A, Sadik A, Sahn F, Gorlia T, Meisner C et al (2020) Methylome analyses of three glioblastoma cohorts reveal chemotherapy sensitivity markers within DDR genes. *Cancer Med* 9:8373–8385. <https://doi.org/10.1002/cam4.3447>
 12. Louis DN, Perry A, Wesseling P, Brat DJ, Cree IA, Figarella-Branger D et al (2021) The 2021 WHO Classification of Tumors of the Central Nervous System: a summary. *Neuro Oncol*. <https://doi.org/10.1093/neuonc/noab106>
 13. Lucas CG, Sloan EA, Gupta R, Wu J, Pratt D, Vasudevan HN et al (2022) Multiplatform molecular analyses refine classification of gliomas arising in patients with neurofibromatosis type 1. *Acta Neuropathol*. <https://doi.org/10.1007/s00401-022-02478-5>
 14. Mackay A, Burford A, Molinari V, Jones DTW, Izquierdo E, Brouwer-Visser J et al (2018) Molecular, pathological, radiological, and immune profiling of non-brainstem pediatric high-grade glioma from the HERBY Phase II Randomized Trial. *Cancer Cell* 33(829–842):e825. <https://doi.org/10.1016/j.ccell.2018.04.004>
 15. Min JL, Hemani G, Davey Smith G, Relton C, Suderman M (2018) Meffil: efficient normalization and analysis of very large DNA methylation datasets. *Bioinformatics* 34:3983–3989. <https://doi.org/10.1093/bioinformatics/bty476>
 16. Pajtler KW, Witt H, Sill M, Jones DT, Hovestadt V, Kratochwil F et al (2015) Molecular classification of ependymal tumors across all CNS compartments, histopathological grades, and age groups. *Cancer Cell* 27:728–743. <https://doi.org/10.1016/j.ccell.2015.04.002>
 17. Parker KA, Robinson NJ, Schiemann WP (2022) The role of RNA processing and regulation in metastatic dormancy. *Semin Cancer Biol* 78:23–34. <https://doi.org/10.1016/j.semcancer.2021.03.020>
 18. Pratt D, Abdullaev Z, Papanicolaou-Sengos A, Ketchum C, Panneer Selvam P, Chung HJ et al (2022) High-grade glioma with pleomorphic and pseudopapillary features (HPAP): a proposed type of circumscribed glioma in adults harboring frequent TP53 mutations and recurrent monosomy 13. *Acta Neuropathol* 143:403–414. <https://doi.org/10.1007/s00401-022-02404-9>
 19. Pratt D, Lucas CG, Selvam PP, Abdullaev Z, Ketchum C, Quezado M et al (2022) Recurrent ACVR1 mutations in posterior fossa ependymoma. *Acta Neuropathol* 144:373–376. <https://doi.org/10.1007/s00401-022-02435-2>
 20. Raffeld M, Abdullaev Z, Pack SD, Xi L, Nagaraj S, Briceno N et al (2020) High level MYCN amplification and distinct methylation signature define an aggressive subtype of spinal cord ependymoma. *Acta Neuropathol Commun* 8:101. <https://doi.org/10.1186/s40478-020-00973-y>
 21. Reinhardt A, Stichel D, Schrimpf D, Koelsche C, Wefers AK, Ebrahimi A et al (2019) Tumors diagnosed as cerebellar glioblastoma comprise distinct molecular entities. *Acta Neuropathol Commun* 7:163. <https://doi.org/10.1186/s40478-019-0801-8>
 22. Reinhardt A, Stichel D, Schrimpf D, Sahn F, Korshunov A, Reuss DE et al (2018) Anaplastic astrocytoma with piloid features, a novel molecular class of IDH wildtype glioma with recurrent MAPK pathway, CDKN2A/B and ATRX alterations. *Acta Neuropathol* 136:273–291. <https://doi.org/10.1007/s00401-018-1837-8>
 23. Ren X, Kuan PF (2019) methylGSA: a bioconductor package and Shiny app for DNA methylation data length bias adjustment in gene set testing. *Bioinformatics* 35:1958–1959. <https://doi.org/10.1093/bioinformatics/bty892>
 24. Robinson JT, Thorvaldsdottir H, Wenger AM, Zehir A, Mesirov JP (2017) Variant review with the integrative genomics viewer. *Cancer Res* 77:e31–e34. <https://doi.org/10.1158/0008-5472.CAN-17-0337>
 25. Singh O, Pratt D, Aldape K (2021) Immune cell deconvolution of bulk DNA methylation data reveals an association with methylation class, key somatic alterations, and cell state in glial/glioneuronal tumors. *Acta Neuropathol Commun* 9:148. <https://doi.org/10.1186/s40478-021-01249-9>
 26. Stanley RF, Abdel-Wahab O (2022) Dysregulation and therapeutic targeting of RNA splicing in cancer. *Nat Cancer* 3:536–546. <https://doi.org/10.1038/s43018-022-00384-z>
 27. Sturm D, Orr BA, Toprak UH, Hovestadt V, Jones DTW, Capper D et al (2016) New brain tumor entities emerge from molecular classification of CNS-PNETs. *Cell* 164:1060–1072. <https://doi.org/10.1016/j.cell.2016.01.015>
 28. Sturm D, Witt H, Hovestadt V, Khuong-Quang DA, Jones DT, Konermann C et al (2012) Hotspot mutations in H3F3A and IDH1 define distinct epigenetic and biological subgroups of glioblastoma. *Cancer Cell* 22:425–437. <https://doi.org/10.1016/j.ccr.2012.08.024>
 29. Tanguturi SK, Trippa L, Ramkissoon SH, Pelton K, Knoff D, Sandak D et al (2017) Leveraging molecular datasets for biomarker-based clinical trial design in glioblastoma. *Neuro Oncol* 19:908–917. <https://doi.org/10.1093/neuonc/now312>
 30. Thomas C, Sill M, Ruland V, Witten A, Hartung S, Kordes U et al (2016) Methylation profiling of choroid plexus tumors reveals 3 clinically distinct subgroups. *Neuro Oncol* 18:790–796. <https://doi.org/10.1093/neuonc/nov322>

31. Yang B, Wang JQ, Tan Y, Yuan R, Chen ZS, Zou C (2021) RNA methylation and cancer treatment. *Pharmacol Res* 174:105937. <https://doi.org/10.1016/j.phrs.2021.105937>

Publisher's Note Springer Nature remains neutral with regard to jurisdictional claims in published maps and institutional affiliations.

Authors and Affiliations

Patrick J. Cimino¹  · Courtney Ketchum² · Rust Turakulov² · Omkar Singh² · Zied Abdullaev² · Caterina Giannini³ · Peter Pytel⁴ · Giselle Yvette Lopez⁵ · Howard Colman⁶ · MacLean P. Nasrallah⁷ · Mariarita Santi⁸ · Igor Lima Fernandes⁹ · Jeff Nirschl¹⁰ · Sonika Dahiya¹¹ · Stewart Neill¹² · David Solomon¹³ · Eilis Perez¹⁴ · David Capper¹⁴ · Haresh Mani¹⁵ · Dario Caccamo¹⁶ · Matthew Ball¹⁷ · Michael Badruddoja¹⁸ · Rati Chkheidze¹⁹ · Sandra Camelo-Piragua²⁰ · Joseph Fullmer²¹ · Sanda Alexandrescu²² · Gabrielle Yeany²³ · Charles Eberhart²⁴ · Maria Martinez-Lage²⁵ · Jie Chen²⁶ · Leor Zach²⁷ · B. K. Kleinschmidt-DeMasters²⁸ · Marco Hefti²⁹ · Maria-Beatriz Lopes³⁰ · Nicholas Nuechterlein³¹ · Craig Horbinski³² · Fausto J. Rodriguez³³ · Martha Quezado² · Drew Pratt² · Kenneth Aldape²

¹ Surgical Neurology Branch, National Institute of Neurological Disorders and Stroke, National Institutes of Health, 10 Center Dr., Room 3D20, Bethesda, MD 20892, USA

² Laboratory of Pathology, Center for Cancer Research, National Cancer Institute, National Institutes of Health, 10 Center Dr., Room 2S235, Bethesda, MD 20892, USA

³ Department of Laboratory Medicine and Pathology, Mayo Clinic, Rochester, MN, USA

⁴ Department of Pathology, University of Chicago, Chicago, IL, USA

⁵ Department of Pathology, Duke University, Durham, NC, USA

⁶ Department of Neurosurgery, Huntsman Cancer Institute, University of Utah, Salt Lake City, UT, USA

⁷ Department of Pathology and Laboratory Medicine, Perelman School of Medicine, University of Pennsylvania, Philadelphia, PA, USA

⁸ Department of Pathology and Laboratory Medicine, Children's Hospital of Philadelphia, Philadelphia, PA, USA

⁹ Laboratório Bacchi, São Paulo, Brazil

¹⁰ Department of Pathology, Stanford University, Stanford, CA, USA

¹¹ Department of Pathology and Immunology, Washington University, St. Louis, MO, USA

¹² Department of Pathology and Laboratory Medicine, Emory University, Atlanta, GA, USA

¹³ Department of Pathology, University of California San Francisco, San Francisco, CA, USA

¹⁴ Charité, Universitätsmedizin Berlin, Berlin, Germany

¹⁵ Department of Pathology, Inova Fairfax Hospital, Fairfax, VA, USA

¹⁶ Department of Pathology, Mercy General Hospital, Sacramento, CA, USA

¹⁷ Department of Neurology, Center for Neurosciences, Tucson, AZ, USA

¹⁸ Department of Pathology, Tucson Medical Center, Tucson, AZ, USA

¹⁹ Department of Pathology, University of Alabama, Birmingham, AL, USA

²⁰ Department of Pathology, University of Michigan Medical Center, Ann Arbor, MI, USA

²¹ Department of Pathology, Beaumont Hospital, Royal Oak, MI, USA

²² Department of Pathology, Boston Children's Hospital, Boston, MA, USA

²³ Department of Pathology, Cleveland Clinic, Cleveland, OH, USA

²⁴ Department of Pathology, Johns Hopkins Hospital, Baltimore, MD, USA

²⁵ Department of Pathology, Massachusetts General Hospital, Boston, MA, USA

²⁶ Department of Pathology and Microbiology, University of Nebraska Medical Center, Omaha, NE, USA

²⁷ Sackler Faculty of Medicine, Tel Aviv University, Tel Aviv, Israel

²⁸ Department of Pathology, University of Colorado Hospital, Aurora, CO, USA

²⁹ Department of Pathology, University of Iowa Hospitals, Iowa City, IA, USA

³⁰ Department of Pathology, University of Virginia Health System, Charlottesville, VA, USA

³¹ Paul G. Allen School of Computer Science & Engineering, University of Washington, Seattle, WA, USA

³² Department of Pathology, Northwestern Memorial Hospital, Chicago, IL, USA

³³ Department of Pathology, University of California Los Angeles Medical Center, Los Angeles, CA, USA